HHS Public Access

Author manuscript

J Hypertens. Author manuscript; available in PMC 2019 October 01.

Published in final edited form as:

J Hypertens. 2019 October ; 37(10): 2061–2073. doi:10.1097/HJH.0000000000002129.

Coexisting renal artery stenosis and metabolic syndrome magnifies mitochondrial damage, aggravating post-stenotic kidney injury in pigs

Arash AGHAJANI NARGESI, MD, MPH[a], **Lihong ZHANG, MD**[a,b], **Hui TANG, MD, PhD**[a], **Kyra L. JORDAN**[a], **Ishran M. SAADIQ**[a], **Stephen C. TEXTOR, MD**[a], **Lilach O. LERMAN, MD, PhD**[a], **Alfonso EIRIN, MD**[a]

[a]Department of Internal Medicine, Division of Nephrology and Hypertension, Mayo Clinic, Rochester, MN

[b]Department of Nephrology, the Fifth People's Hospital of Shanghai, Fudan University, Shanghai 200240, China

Abstract

Objective: Renovascular disease (RVD) produces chronic underperfusion of the renal parenchyma and progressive ischemic injury. Metabolic abnormalities often accompany renal ischemia, and are linked to poorer renal outcomes. However, the mechanisms of injury in kidneys exposed to the ischemic and metabolic components of RVD are incompletely understood. We hypothesized that coexisting renal artery stenosis (RAS) and metabolic syndrome (MetS) would exacerbate mitochondrial damage, aggravating post-stenotic kidney injury in swine.

Methods: Domestic pigs were studied after 16 weeks of either standard diet (Lean) or high-fat/high-fructose (MetS) with or without superimposed RAS (n=6 each). Single-kidney renal blood flow (RBF) and glomerular filtration rate (GFR) were assessed in-vivo with multi-detector-CT, and renal tubular mitochondrial structure, homeostasis and function and renal injury ex-vivo.

Results: Both RAS groups achieved significant stenosis. Single-kidney RBF and GFR were higher in MetS compared to Lean, but decreased in Lean+RAS and MetS+RAS versus their respective controls. MetS and RAS further induced changes in mitochondrial structure, dynamics, and function, and their interaction (diet x ischemia) decreased matrix density, mitophagy, and ATP production, and lead to greater renal fibrosis.

Conclusion: Coexisting RAS and MetS synergistically aggravate mitochondrial structural damage and dysfunction, which may contribute to structural injury and dysfunction in the post-stenotic kidney. These observations suggest that mitochondrial damage precedes loss of renal

Correspondence: Alfonso Eirin, MD, Division of Nephrology and Hypertension, Mayo Clinic, 200 First Street SW, Rochester, MN, 55905. eirinmassat.alfonso@mayo.edu, Phone: (507)-538-9941, Fax: (507)-266-9316.

This study has not been published and is not being considered for publication elsewhere in whole or in part in any language except as an abstract.

Conflict of Interest

None.

The authors declared no potential conflicts of interest with respect to the research, authorship, and/or publication of this article.

function in experimental RVD, and position mitochondria as novel therapeutic targets in these patients.

Keywords

Renovascular disease; Renal artery stenosis; Metabolic syndrome; Mitochondria; Hypertension

Introduction

Renovascular disease (RVD) accounts for an important proportion of secondary hypertension and is increasingly associated with progressive renal dysfunction and cardiovascular complications[1]. In RVD, the progressive narrowing of the renal artery produces chronic underperfusion of the renal parenchyma, and ischemic injury often designated as 'ischemic nephropathy'[2, 3]. Metabolic abnormalities, including obesity, hyperlipidemia, and insulin resistance, often accompany renal ischemia in the clinical setting, and are linked to poorer outcomes after renal revascularization[4]. Alas, elucidation of the mechanisms responsible for ongoing renal injury in RVD is critical to prevent its progression and develop novel therapies to treat this prevalent disease.

Renal tubular cells are highly dependent on adequate function of their mitochondria[5], which produce 90% of cellular energy in the form of adenosine triphosphate (ATP), but also regulate numerous cellular functions, including proliferation, survival, and death[6]. These organelles are highly dynamic, and their functions rely on the continuous balance of biogenesis, fusion, fission, and degradation (mitophagy). Mitochondria are also the main source of reactive oxygen species (ROS), and their excessive formation may subsequently damage both mitochondrial and cell constituents. Therefore, mitochondrial injury may impair overall tubular cell function[7].

We have previously shown that surgically-induced renal artery stenosis (RAS) in swine induces tubular cell mitochondrial damage in the stenotic kidney, associated with hypoxia, oxidative stress, and fibrosis[8, 9]. We have also shown that renal tubular cells from pigs with diet-induced metabolic syndrome (MetS) exhibit significant renal mitochondrial structural abnormalities and dysfunction, associated with renal oxidative stress, tubular injury, and fibrosis[10]. RAS[11, 12] and MetS[13, 14] alone are also associated with cardiac mitochondrial structural and functional damage in pigs. However, whether coexisting MetS and RAS magnifies mitochondrial damage remains unknown.

This study employed a novel large animal model of MetS+RAS[7, 15] that closely mimics the coexistence of the ischemic and metabolic components of human RVD to test the hypothesis that concurrent MetS and RAS exacerbates mitochondrial damage, aggravating post-stenotic kidney injury in swine.

Materials and methods

The Institutional Animal Care and Use Committee approved this study. Twenty-four 3-month old female domestic pigs were studied for 16 weeks (Figure 1). We opted to use female pigs to test whether the deleterious effects on MetS and RAS on the kidney outweigh

gender-specific protection[16, 17]. At baseline, animals were randomized into two groups, which were fed either a high-cholesterol/high-carbohydrate diet (MetS) containing (in % kcal) 17% protein, 20% complex carbohydrates, 20% fructose, and 43% fat and supplemented with 2% cholesterol and 0.7% sodium cholate by weight)[18] or standard pig chow (Lean) for the duration of the study.

Six weeks later, animals were anesthetized with 0.25g of IM tiletamine hydrochloride/ zolazepam hydrochloride (Telazol®, Fort Dodge Animal Health, New York) and 0.5g of xylazine, and maintained with intravenous ketamine (0.2mg/kg/min) and xylazine (0.03mg/kg/min). RAS was induced in 6 MetS and 6 Lean pigs by placing an irritant coil in the main renal artery using fluoroscopy, a procedure that gradually develops unilateral RAS within 1–2 weeks[19]. A sham procedure, which involves cannulating the renal artery (without placement of irritant coil) and selective renal angiography with contrast injections, was performed in the remaining 6 Lean and 6 MetS pigs.

Ten weeks later, animals were similarly anesthetized and the degree of stenosis in each animal was determined by angiography. Systemic blood samples were collected and lipid panels (enzyme immunoassay kit, Roche Diagnostics, Indianapolis), plasma renin activity (PRA, GammaCoat kit; DiaSorin), serum creatinine[20], and fasting glucose and insulin levels were measured by standard procedures. Insulin resistance was assessed by the homeostasis model assessment of insulin resistance (HOMA-IR)[18]. Urine samples were also collected and albumin creatinine ratio (ACR) calculated. Single-kidney hemodynamics and function were assessed using multi-detector computed tomography (MDCT), and blood pressure measured with an 8 French intra-arterial catheter during MDCT studies[21].

Three days later, animals were euthanized with an i.v. bolus of 100mg/kg of sodium pentobarbital (Fatal-Plus, Vortech Pharmaceuticals, Dearborn). Stenotic kidneys and hearts were harvested, and sections frozen in liquid nitrogen (and maintained at −80°C) or preserved in formalin or Trump’s fixative for ex-vivo studies.

In-vivo studies

Single-kidney volume, renal blood flow (RBF), and glomerular filtration rate (GFR) were assessed using a Flash 128 MDCT scanner (Somatom Definition Flash, Siemens Healthcare), as previously described[21, 22]. After a bolus of iopamidol (0.5cc/kg/2s), 70 multi-scan exposures were acquired at a cycle time of 0.67sec (flow study), followed by 70 scans at a cycle time of 2sec. Volume images were reconstructed and initiation of acquisition set to trigger near the peak of the aorta intensity signal. The duration of acquisition time encompassed the vascular phase of contrast through the cortex of the kidneys (maximal intensity). Regions of interest were selected from cross-sectional images from the aorta, renal cortex, and medulla. Average tissue attenuation curves were fitted by curve-fitting algorithms to calculate hemodynamics in cortical and medullary regions of the kidney. Cortical and medullary volumes were calculated by planimetry (Analyze, Biomedical Imaging Resource, Mayo Clinic, Rochester, Minnesota). Single-kidney GFR was calculated from the cortical curve slope and RBF by multiplying kidney volume (ml of tissue) by renal perfusion (ml/min per ml of tissue), as previously described[23, 24]. Visceral fat volume was

traced in 15 abdominal slides around the middle level of kidney on MDCT images, and expressed as volume and fraction, as previously described[18, 25–28].

Ex-vivo studies

Renal Mitochondrial Structure—Renal mitochondrial density was examined by immunofluorescence staining with the mitochondrial outer membrane marker preprotein translocases of the outer membrane (TOM)-20 (Santa Cruz Biotechnology, Catalog#: sc-11415, Dallas, TX) and quantified in 15–20 random fields using a computer-aided image analysis program (ZEN 2012 blue edition, Carl ZEISS SMT; Oberkochen, Germany).

Mitochondrial morphology was assessed in renal samples using digital electron microscopy (Phillips CM10 Transmission Electron Microscopy) and processed at the Mayo Clinic's electron microscopy core facility. Stenotic kidney sections were preserved in Trump's fixative and mounted on mesh grids, stained with aqueous uranyl acetate and lead citrate. For analysis, five representative tubular cells from 5 different tubules and 5 representative glomeruli were randomly selected. Tubular cells and podocytes were identified visually by well-recognized characteristics of cell diameter, shape, and size. Tubular cell and podocyte mitochondrial area, perimeter, and matrix density were measured in 5 representative mitochondria in these cells using Image-J (Version 1.5, National institute of Health)[29], and the results averaged per pig.

Renal Mitochondrial homeostasis and function—Mitochondrial biogenesis was evaluated by renal expression of peroxisome proliferator activated receptor-γ-coactivator (PGC)-1α (Abcam, 1:1000, Catalog#: ab72230, Cambridge, United Kingdom). Mitochondrial fusion and fission were assessed by the expression of mitofusin (MFN)-2 (Cell signaling, 1:1000, Catalog#: 9482, Danvers, MA) and dynamin-related protein (DRP)-1 (Cell signaling, 1:1000, Catalog#: 8570, Danvers, MA), respectively. Mitophagy was measured by renal expression of BCL2 interacting protein (BNIP)-3 (Bioss, Catalog#: bs-4239R, Woburn, MA) and double immunofluorescence staining with TOM-20 and parkin (Santa Cruz, Catalog#: sc-13279, Dallas, TX). The extent of co-localization between TOM-20 and parkin was assessed with the Mander's overlap coefficient using Image-J (Co-localization Plugin) and reported as M1 (representing overlap between Parkin and TOM-20)[13, 30].

In addition, mitochondria were isolated using the MITO-ISO kit (Catalog #8268, ScienCell, Carlsbad, California)[31]. Frozen kidney tissue (10mg) was resuspended in assay buffer (100μl) and homogenized (10–15 passes). Samples were then centrifuged (13226g for 5min) in a microcentrifuge, and the supernatant collected. Deproteinization steps were followed according to manufacture protocol. A total of 50μl of deproteinized samples were added into the plate and read at OD570nm. Mitochondrial hydrogen peroxide (H_20_2) production, cytochrome-c oxidase (COX)-IV activity, and ATP/ADP levels were measured by colorimetric quantitative methods (OxisResearch, BIOXYTECH® H_20_2-560™ Assay, Cat# 21024, and abcam, Cat# ab83355, Cambridge, United Kingdom, respectively)[32].

Renal injury—Renal production of superoxide anion was evaluated by fluorescence microscopy using dihydroethidium (DHE)[33]. Tubular injury was scored in a blinded fashion

in sections stained with Periodic acid-Schiff, as previously described[9, 34]. Absence of brush border, dilation, atrophy, cast formation, cell detachment, or thickening of tubular basement membrane were scored from 1 to 5 (0 being normal tubules, 1: <10% of tubules injured, 2: 10–25% of tubules injured, 3: 26–50% of tubules injured, 4: 51–75% of tubules injured, 5: >75% of tubules injured). Tubulointerstitial fibrosis was assessed in midhilar renal cross-sections stained with trichrome, semi-automatically quantified in 15–20 fields, expressed as fraction of kidney surface area, and the results from all fields averaged. Glomerular score (% of sclerotic out of 100 glomeruli) was also assessed.

Cardiac mitochondrial structure—Myocardial mitochondria were examined by transmission electron microscopy, as previously described[13]. For analysis, five representative cardiomyocytes were randomly selected in each pig myocardium. Mitochondrial area, perimeter, and matrix density were measured using Image-J, and the results were averaged per pig.

Statistical analysis—Statistical analysis was performed using JMP (SAS) software. Results were expressed as mean ± SD or median (interquartile range). The Shaphiro-Wilk test was used to test for deviation from normality. Analysis of variance (ANOVA) and Student's t-test were used to compare normally distributed parameters, whereas those that did not follow a Gaussian distribution were compared using nonparametric methods (Wilcoxon or Kruskal-Wallis). Two-way ANOVA was performed to analyze the effects of RAS and MetS as separate factors, and their interactions, followed by Tukey's test as appropriate. For variables with non-normal distributions, log-transformed values were used for two-way ANOVA. Results were considered significant for $p<0.05$.

Results

Systemic characteristics and renal function in study groups are summarized in Table 1. Body weight and visceral fat volume (Figure S1) were similarly elevated in MetS and MetS+RAS groups compared to their respective controls. Blood pressure was equally elevated in MetS, Lean+RAS, and MetS+RAS. All RAS pigs developed moderate, but significant stenosis of a similar degree. Lipid fractions were higher in MetS groups compared Lean groups, as were fasting insulin and HOMA-IR score. Yet, glucose levels did not differ among the groups, indicating non-diabetic MetS. Serum creatinine was higher in Lean+RAS compared to Lean and MetS pigs, but further increased in MetS+RAS. However, PRA did not differ among the groups, as typical to the chronic phase of untreated RAS[35]. ACR was similarly higher in Lean+RAS and MetS+RAS compared to Lean and MetS, and influenced only by ischemia. Single-kidney volume, RBF, and GFR were higher in MetS compared to Lean pigs, indicating hyperfiltration, but decreased in the stenotic Lean+RAS and MetS+RAS kidneys compared to their respective controls. A 2-way ANOVA analysis revealed that renal volume, RBF, and GFR were all increased by diet and decreased by the stenosis, so that overall coexistence of MetS diet and ischemia did not measurably aggravate stenotic-kidney hemodynamics and function (Table 1, $p>0.05$ all). Renal volume, RBF and GFR differences between Lean+RAS and MetS+RAS and their respective controls remained significant after adjustment by body weight (all $p<0.05$), but did not differ between Lean and MetS+RAS.

MetS+RAS aggravates renal mitochondrial structural damage

Mitochondrial density was similarly lower in Lean+RAS and MetS+RAS compared to Lean and MetS pigs, reflected in decreased renal immunoreactivity of the mitochondrial marker TOM-20 (Figure 2A). Transmission electron microscopy revealed that renal tubular mitochondrial area and perimeter increased in MetS and Lean+RAS compared to Lean, and further increased in MetS+RAS (Figure 2B). Contrarily, mitochondrial matrix density that decreased in MetS and Lean+RAS versus Lean further decreased in MetS+RAS, accompanied by loss of cristae structure, and the interaction of MetS diet and ischemia synergistically decreased matrix density (Figure 2C, $p<0.01$, 2-way ANOVA). Tubular epithelial cell mitochondrial from MetS+RAS pigs exhibit outer membrane disruption, and release of mitochondrial content into the cytosol (Figure S2). Podocyte mitochondrial density was similarly decreased in MetS, Lean+RAS, and MetS+RAS compared to Lean, and influenced only by ischemia (Figure 3A). Mitochondrial area, perimeter, and matrix density were lower in MetS compared to Lean, but the latter further decreased in Lean+RAS and MetS+RAS, and was influenced by MetS diet, ischemia, and their interaction.

MetS+RAS alters renal mitochondrial homeostasis

Renal expression of PGC-1α was similar among the groups, indicating preserved mitochondrial biogenesis (Figure 4A). Renal expression of the fusion marker MFN-2 increased in MetS compared to Lean, but decreased in Lean+RAS and MetS+RAS compared to their respective controls (Figure 4B). Renal expression of the fission marker DRP-1 remained unchanged in MetS, but similarly decreased in Lean+RAS and MetS+RAS (Figure 4C). The interaction of MetS diet and ischemia did not affect either mitochondrial biogenesis or dynamics ($p>0.05$, 2-way ANOVA).

Renal parkin expression and its co-localization with TOM-20 were similar between Lean and MetS, but increased in Lean+RAS and MetS+RAS groups, as did renal expression of marker BNIP-3, implying increased mitophagy (Figure 5A–B). Defective parkin and TOM-20 co-localization was associated with the effect of ischemia, and decreased BNIP-3 expression also with the interaction of MetS diet x ischemia ($p>0.01$, 2-way ANOVA). Transmission electron microscopy showed clusters of structurally damaged mitochondria in the vicinity of the nucleus of Lean+RAS and MetS+RAS tubular epithelial cells (Figure 5C), some of which appeared to be engulfed within mitophagosomes (Figure 5D).

MetS+RAS exacerbates renal mitochondrial dysfunction

Production of H_20_2 in isolate mitochondria was elevated in MetS and MetS+RAS compared to Lean and Lean+RAS groups, suggesting increased mitochondrial oxidative stress (Figure 6A). Mitochondrial COX-IV activity decreased in MetS compared to Lean, and further decreased in Lean+RAS and MetS+RAS (Figure 6C). ATP generation similarly decreased in MetS and Lean+RAS compared to Lean, and further decreased in MetS+RAS (Figure 6B). The interaction of MetS diet and ischemia exacerbated the impairment of ATP production ($p<0.05$, 2-way ANOVA).

MetS+RVD magnifies renal injury

Renal superoxide anion production and tubular injury increased in MetS and Lean+RAS compared to Lean, and further increased in MetS+RAS (Figure 7A–B). Tubulo-interstitial fibrosis was similar between Lean and MetS, increased in Lean+RAS, and further increased in MetS+RAS (Figure 7C). The interaction of MetS diet and ischemia magnified renal fibrosis (p=0.002, 2-way ANOVA). Glomerular score was higher in Lean+RAS versus Lean and MetS, further increased in MetS+RAS, and was influenced by MetS diet, ischemia, and their interaction (Figure 3B).

Renal ischemia induces cardiac mitochondrial structural damage

Myocardial mitochondrial density, area, and perimeter did not differ among the groups, but matrix density was similarly decreased in Lean+RAS and MetS+RAS compared to their respective controls, and influenced only by ischemia (Figure S3).

Discussion

The current study shows that coexisting RAS and MetS amplify renal tubular mitochondrial damage and impair energy production in the post-stenotic kidney. The interaction of MetS diet and ischemia increased mitophagy, decreased matrix density and ATP production, and led to greater renal fibrosis. Therefore, RAS and MetS synergize and magnify their adverse effects on the post-ischemic kidney, enhancing tubular mitochondrial damage and tissue injury. Given that renal dysfunction was not magnified in MetS+RAS, these observations suggest that mitochondrial damage precedes loss of renal function, and may imply that mitoprotective strategies might be useful for patients suffering this prevalent disease.

RVD remains a prevalent condition among the elderly population, associated with accelerated renal injury, hypertension, and several cardiovascular complications. The prevalence of RVD is high in patients referred for coronary angiography[36], and it often accompanies coronary artery disease, carotid artery stenosis, or peripheral artery disease[37, 38]. While progressive reduction of renal perfusion leads to ischemic injury, atherosclerosis and metabolic abnormalities may activate additional pathogenic factors and aggravate renal damage. In line with this notion, patients with concomitant RAS and MetS have few renal benefits following endovascular intervention[4], suggesting that the interaction of MetS diet and ischemia may accentuate post-stenotic injury.

We have previously shown that RAS in swine induces tubular cell mitochondrial damage in the stenotic kidney, associated with renal hypoxia, oxidative stress, and fibrosis[8, 9]. We have also shown that renal tubular cells from pigs with MetS exhibit significant mitochondrial structural abnormalities and dysfunction, associated with renal oxidative stress and tubular injury[10]. The current study extends our previous observations and shows that coexisting MetS and RAS in fact magnify mitochondrial damage in the post-stenotic kidney in swine. Specifically, we found that TOM-20 immunoreactivity was preserved in MetS pigs, but similarly decreased in both RAS groups, suggesting that decreased mitochondrial density in this model may be attributed mainly to the ischemia. Tubular cell mitochondrial area and perimeter were higher in MetS, RAS, and MetS+RAS, but both were affected only by diet

and ischemia alone, arguing against a major additional impact of MetS on renal tubular cell mitochondrial shape in RAS.

The swollen appearance of these mitochondria possibly reflects the influx of water into the organelle. The inner mitochondrial membrane is a major barrier for the movement of solutes and water between cytosol and mitochondria, and the osmotic balance between these two compartments regulates mitochondrial matrix volume[39, 40]. Increased mitochondrial permeability facilitate water entry into the matrix, which compresses cristae membranes, altering the topology of the inner mitochondrial membrane[41]. In agreement, we found that tubular cell mitochondrial matrix density decreased in MetS and Lean+RAS, and further decreased in MetS+RAS, underscoring the synergistic contribution of MetS diet and ischemia on tubular cell mitochondrial structural damage. Contrarily, MetS+RAS-induced mitochondrial damage in podocytes evidently resulted primarily from the effect of ischemia. We found that podocyte mitochondrial area, perimeter, and matrix density were lower in MetS compared to Lean, but the latter further decreased in Lean+RAS and MetS+RAS. In line with this, ACR was similarly elevated in Lean+RAS and MetS+RAS compared to Lean and MetS, and influenced only by ischemia.

It is possible that coexisting ischemia and MetS exacerbates renal oxidative stress, compromising the integrity of the inner mitochondrial membrane. We have shown in swine that both RAS[8] and MetS[10] trigger peroxidation and loss of the inner mitochondrial membrane phospholipid cardiolipin, increasing mitochondrial permeability and swelling. Excessive mitochondrial swelling ultimately leads to disruption of the outer membrane and release of mitochondrial matrix content into the cytosol, as we observed in tubular cell mitochondria from MetS+RAS pigs.

In addition, we found that the ischemic and metabolic components of RVD interfere with mitochondrial homeostasis, a finely balanced network of quality control pathways that regulate mitochondrial formation, shape, and degradation[42]. Mitochondrial biogenesis, the process of formation of new mitochondria, remained unchanged, disclosed by unaltered expression of PGC-1α, the master regulator of this pathway[43]. Although renal expression of the fusion marker MFN-2 was influenced by the individual effect of diet and ischemia, expression of DRP-1, which induces mitochondrial fragmentation[44], was affected only by ischemia. Fusion and fission play a key role in modulating mitochondrial morphology[45]. MetS-induced activation of mitochondrial fusion might have contributed to increase mitochondrial area and perimeter. However, RAS- induced changes in mitochondrial dynamics were not consistent with changes in mitochondrial shape. Therefore, mitochondrial swelling in RAS groups may result from alterations in osmotic balance or inner membrane permeability rather than changes in fusion or fission.

Interestingly, we found that mitophagy, the removal of damaged mitochondria through autophagy[46], was primarily affected by ischemia and amplified by its interaction with MetS diet. Although mitophagy is considered a mechanism of cellular protection, disproportional activation of this pathway may lead to mitochondrial remodeling, decreased biogenetic capacity, and cell death[47–49]. Parkin is an E3 ubiquitin ligase that is recruited to the outer mitochondrial membrane where selectively binds only to damaged mitochondria, inducing

mitophagy[50]. Here we found that RAS recruited parkin to renal tubular cell mitochondria, disclosed by its co-localization with the outer membrane protein TOM-20 and increased expression of BNIP-3, a mitochondrial protein that facilitates parkin recruitment[51]. This correlates with previous in-vitro and in-vivo studies showing that both diet-induced obesity[52] and hypoxia[53] can increase BNIP-3 abundance, promoting mitophagy. Parkin has been also implicated in the transport of damaged mitochondria along microtubules to the perinuclear region[54]. In line with this, we found that a significant number of damaged mitochondria from Lean+RAS and MetS+RAS pigs were localized in the vicinity of the nucleus. Moreover, we identified several mitochondria from RAS groups engulfed by autophagosomes (mitophagosome), likely destined for degradation.

Mitochondria H_20_2 production can oxidatively damage mitochondrial lipids and DNA, as well as electron transport chain proteins, impairing ATP synthesis[55]. In addition to increased mitochondrial oxidative stress, we found that MetS diet and ischemia impaired the activity of COX-IV, which catalyzes the final step in mitochondrial electron transfer chain[56], and their interaction (diet x ischemia) decreased ATP production. Taken together, these observations suggest that coexisting RAS and MetS aggravated renal mitochondrial structural damage and dysfunction.

The mechanisms by which MetS and RAS synergistically interact to impair renal mitochondrial structure and function are multifactorial and may include generating a vicious cycle of renal hypoxia, oxidative stress, and apoptosis, among others. Renal hypoxia is a common finding in severe swine[8] and human[57] RAS, and is associated with lower perfusion, RBF, and GFR. Concurrent nutrient surplus typical of MetS can then magnify renal hypoxia by increasing tubular oxygen consumption[10] and amplifying tubulointerstitial fibrosis[7]. Hypoxia directly affects mitochondria by decreasing electron-transport rate and increasing ROS generation[58]. Furthermore, hypoxia-induced mitochondrial injury upregulates the expression of BNIP-3, promoting mitophagy[59], in line with our observations in MetS+RAS pigs.

Hyperglycemia can also alter the metabolic profile of both mesangial and tubular cells by reducing their mitochondrial respiratory function[60]. Likewise, cultured vascular endothelial cells exposed to hyperglycemic glucose concentrations produce enhanced levels of superoxide, which are significantly attenuated by mitoprotection[61]. Therefore, hyperglycemia may exacerbate obesity- and hypertension-induced mitochondrial damage. However, we found that glucose levels were similar among the groups, arguing against a major detrimental effect of hyperglycemia on mitochondrial structure and function in our model.

RAS is also accompanied by significant systemic and renal oxidative stress, which can damage several constituents of tubular cell mitochondria[8, 62]. We have shown in swine RAS that peroxidation and loss of cardiolipin secondary to ischemia triggers mitochondrial ROS production and oxidative stress[8, 9]. MetS induces renal tubular cell lipid accumulation and cardiolipin peroxidation[10] likely amplifying mitochondrial injury in the post-stenotic kidney. Renal adiposity and apoptosis also interfere with mitochondrial fatty acid β-oxidation,

exacerbating cellular lipid accumulation and creating a vicious cycle of lipid toxicity and mitochondrial injury[63, 64].

Importantly, MetS and RAS-induced mitochondrial abnormalities and dysfunction contributed to renal oxidative stress, possibly secondary to the release of mitochondrial ROS to the cytosol. Impaired mitochondrial bioenergetics in MetS and RAS could have led to tubular injury by inducing cytoskeletal abnormalities, membrane defects, and phospholipid breakdown, as commonly observed in ATP-depleted tubular cells[65]. Lastly, coexisting MetS and RAS magnified renal fibrosis, but their interaction did not alter renal hemodynamics and function, suggesting that mitochondrial-independent pathways could have contributed to renal dysfunction in MetS+RAS. Interestingly, renal hemodynamics and function did not differ between Lean and MetS+RAS after adjustment by body weight. Therefore, increased body weight in MetS+RAS, which was associated with hyperfiltration, hyperperfusion, and increases in renal volume, might have counterbalanced RAS-induced loss of renal volume, RBF, and GFR.

Lastly, we found that MetS and RAS also caused mitochondrial damage in the heart. Although myocardial mitochondrial density, area, and perimeter remain unaffected, matrix density similarly decreased in both Lean+RAS and MetS+RAS, and was affected only by ischemia, suggesting that renal ischemia is associated with myocardial structural damage, which is not exacerbated by superimposition of MetS.

Limitations

Our study is limited by the use of relatively young pigs and the short duration of the disease, yet our MetS+RAS model recapitulates the synergistic interaction between the ischemic and metabolic components of human RVD. In addition, our MetS model does not permit discrimination among the effects of individual cardiovascular risk factors like obesity, hypertension, hyperlipidemia, and insulin resistance in the pathogenesis of MetS-induced renal mitochondrial damage. Additional studies are needed to identify specific factors related to ischemia or MetS influencing renal tubular mitochondrial structure and function.

Conclusion

In summary, our study shows that RAS associated with MetS aggravate renal tubular mitochondrial damage and alter mitochondrial homeostasis, blunting ATP production in the stenotic kidney. These pathological alterations were magnified by the interaction of ischemia and MetS diet, accentuating renal fibrosis. Given that renal dysfunction was not magnified in RAS associated with MetS, our observations suggest that mitochondrial damage precedes loss of renal function in experimental RVD. Further studies are needed to test the effectiveness of mitoprotective interventions to attenuate renal injury in MetS+RAS.

Supplementary Material

Refer to Web version on PubMed Central for supplementary material.

Acknowledgments

This work was supported by the NIH grants: DK106427, DK104273, HL123160, DK120292, and DK102325, and by the American Heart Association (18POST34030150).

References

1. Textor SC and Lerman LO. Paradigm Shifts in Atherosclerotic Renovascular Disease: Where Are We Now? J Am Soc Nephrol. 2015;26:2074–80. [PubMed: 25868641]
2. Ritchie J, Green D, Chrysochou C, Chalmers N, Foley RN and Kalra PA. High-risk clinical presentations in atherosclerotic renovascular disease: prognosis and response to renal artery revascularization. Am J Kidney Dis. 2014;63:186–97. [PubMed: 24074824]
3. Zoccali C, Mallamaci F and Finocchiaro P. Atherosclerotic renal artery stenosis: epidemiology, cardiovascular outcomes, and clinical prediction rules. J Am Soc Nephrol. 2002;13 Suppl 3:S179–83. [PubMed: 12466310]
4. Davies MG, Saad WE, Bismuth J, Naoum JJ, Peden EK and Lumsden AB. Impact of metabolic syndrome on the outcomes of percutaneous renal angioplasty and stenting. J Vasc Surg. 2010;51:926–32. [PubMed: 20022208]
5. Pfaller W and Rittinger M. Quantitative morphology of the rat kidney. Int J Biochem. 1980;12:17–22. [PubMed: 7399019]
6. McFarland R, Taylor RW and Turnbull DM. Mitochondrial disease--its impact, etiology, and pathology. Curr Top Dev Biol. 2007;77:113–55. [PubMed: 17222702]
7. Eirin A, Zhu XY, Puranik AS, Tang H, McGurren KA, van Wijnen AJ, Lerman A and Lerman LO. Mesenchymal stem cell-derived extracellular vesicles attenuate kidney inflammation. Kidney Int. 2017;92:114–124. [PubMed: 28242034]
8. Eirin A, Ebrahimi B, Zhang X, Zhu XY, Woollard JR, He Q, Textor SC, Lerman A and Lerman LO. Mitochondrial protection restores renal function in swine atherosclerotic renovascular disease. Cardiovasc Res. 2014;103:461–72. [PubMed: 24947415]
9. Eirin A, Li Z, Zhang X, Krier JD, Woollard JR, Zhu XY, Tang H, Herrmann SM, Lerman A, Textor SC and Lerman LO. A mitochondrial permeability transition pore inhibitor improves renal outcomes after revascularization in experimental atherosclerotic renal artery stenosis. Hypertension. 2012;60:1242–9. [PubMed: 23045468]
10. Eirin A, Woollard JR, Ferguson CM, Jordan KL, Tang H, Textor SC, Lerman A and Lerman LO. The metabolic syndrome induces early changes in the swine renal medullary mitochondria. Transl Res. 2017;184:45–56 e9. [PubMed: 28363084]
11. Eirin A, Williams BJ, Ebrahimi B, Zhang X, Crane JA, Lerman A, Textor SC and Lerman LO. Mitochondrial targeted peptides attenuate residual myocardial damage after reversal of experimental renovascular hypertension. J Hypertens. 2014;32:154–65. [PubMed: 24048008]
12. Eirin A, Ebrahimi B, Kwon SH, Fiala JA, Williams BJ, Woollard JR, He Q, Gupta RC, Sabbah HN, Prakash YS, Textor SC, Lerman A and Lerman LO. Restoration of Mitochondrial Cardiolipin Attenuates Cardiac Damage in Swine Renovascular Hypertension. J Am Heart Assoc. 2016;5.
13. Yuan F, Woollard JR, Jordan KL, Lerman A, Lerman LO and Eirin A. Mitochondrial targeted peptides preserve mitochondrial organization and decrease reversible myocardial changes in early swine metabolic syndrome. Cardiovasc Res. 2018;114:431–442. [PubMed: 29267873]
14. Yuan F, Hedayat AF, Ferguson CM, Lerman A, Lerman LO and Eirin A. Mitoprotection attenuates myocardial vascular impairment in porcine metabolic syndrome. Am J Physiol Heart Circ Physiol. 2018;314:H669–H680. [PubMed: 29196345]
15. Eirin A, Zhu XY, Jonnada S, Lerman A, van Wijnen AJ and Lerman LO. Mesenchymal Stem Cell-Derived Extracellular Vesicles Improve the Renal Microvasculature in Metabolic Renovascular Disease in Swine. Cell Transplant. 2018;27:1080–1095. [PubMed: 29954220]
16. Busserolles J, Mazur A, Gueux E, Rock E and Rayssiguier Y. Metabolic syndrome in the rat: females are protected against the pro-oxidant effect of a high sucrose diet. Exp Biol Med (Maywood). 2002;227:837–42. [PubMed: 12324666]

17. Kauser K and Rubanyi GM. Gender difference in endothelial dysfunction in the aorta of spontaneously hypertensive rats. Hypertension. 1995;25:517–23. [PubMed: 7721392]
18. Pawar AS, Zhu XY, Eirin A, Tang H, Jordan KL, Woollard JR, Lerman A and Lerman LO. Adipose tissue remodeling in a novel domestic porcine model of diet-induced obesity. Obesity (Silver Spring). 2015;23:399–407. [PubMed: 25627626]
19. Lerman LO, Schwartz RS, Grande JP, Sheedy PF and Romero JC. Noninvasive evaluation of a novel swine model of renal artery stenosis. J Am Soc Nephrol. 1999;10:1455–65. [PubMed: 10405201]
20. Eirin A, Zhu XY, Urbieta-Caceres VH, Grande JP, Lerman A, Textor SC and Lerman LO. Persistent kidney dysfunction in swine renal artery stenosis correlates with outer cortical microvascular remodeling. Am J Physiol Renal Physiol. 2011;300:F1394–401. [PubMed: 21367913]
21. Krier JD, Ritman EL, Bajzer Z, Romero JC, Lerman A and Lerman LO. Noninvasive measurement of concurrent single-kidney perfusion, glomerular filtration, and tubular function. Am J Physiol Renal Physiol. 2001;281:F630–8. [PubMed: 11553509]
22. Eirin A, Ebrahimi B, Zhang X, Zhu XY, Tang H, Crane JA, Lerman A, Textor SC and Lerman LO. Changes in glomerular filtration rate after renal revascularization correlate with microvascular hemodynamics and inflammation in Swine renal artery stenosis. Circ Cardiovasc Interv. 2012;5:720–8. [PubMed: 23048054]
23. Eirin A, Saad A, Tang H, Herrmann SM, Woollard JR, Lerman A, Textor SC and Lerman LO. Urinary Mitochondrial DNA Copy Number Identifies Chronic Renal Injury in Hypertensive Patients. Hypertension. 2016;68:401–10. [PubMed: 27324229]
24. Krier JD, Ritman EL, Bajzer Z, Romero JC, Lerman A and Lerman LO. Noninvasive measurement of concurrent single-kidney perfusion, glomerular filtration, and tubular function. Am J Physiol Renal Physiol. 2001;281:F630–8. [PubMed: 11553509]
25. Li Z, Woollard JR, Wang S, Korsmo MJ, Ebrahimi B, Grande JP, Textor SC, Lerman A and Lerman LO. Increased glomerular filtration rate in early metabolic syndrome is associated with renal adiposity and microvascular proliferation. Am J Physiol Renal Physiol. 2011;301:F1078–87. [PubMed: 21775485]
26. Li ZL, Woollard JR, Ebrahimi B, Crane JA, Jordan KL, Lerman A, Wang SM and Lerman LO. Transition from obesity to metabolic syndrome is associated with altered myocardial autophagy and apoptosis. Arterioscler Thromb Vasc Biol. 2012;32:1132–41. [PubMed: 22383702]
27. Zhang X, Li ZL, Woollard JR, Eirin A, Ebrahimi B, Crane JA, Zhu XY, Pawar AS, Krier JD, Jordan KL, Tang H, Textor SC, Lerman A and Lerman LO. Obesity-metabolic derangement preserves hemodynamics but promotes intrarenal adiposity and macrophage infiltration in swine renovascular disease. Am J Physiol Renal Physiol. 2013;305:F265–76. [PubMed: 23657852]
28. Li ZL, Ebrahimi B, Zhang X, Eirin A, Woollard JR, Tang H, Lerman A, Wang SM and Lerman LO. Obesity-metabolic derangement exacerbates cardiomyocyte loss distal to moderate coronary artery stenosis in pigs without affecting global cardiac function. Am J Physiol Heart Circ Physiol. 2014;306:H1087–101. [PubMed: 24508639]
29. Schneider CA, Rasband WS and Eliceiri KW. NIH Image to ImageJ: 25 years of image analysis. Nat Methods. 2012;9:671–5. [PubMed: 22930834]
30. Dunn KW, Kamocka MM and McDonald JH. A practical guide to evaluating colocalization in biological microscopy. Am J Physiol Cell Physiol. 2011;300:C723–42. [PubMed: 21209361]
31. Zhang X, Li ZL, Crane JA, Jordan KL, Pawar AS, Textor SC, Lerman A and Lerman LO. Valsartan regulates myocardial autophagy and mitochondrial turnover in experimental hypertension. Hypertension. 2014;64:87–93. [PubMed: 24752430]
32. Pi J, Bai Y, Zhang Q, Wong V, Floering LM, Daniel K, Reece JM, Deeney JT, Andersen ME, Corkey BE and Collins S. Reactive oxygen species as a signal in glucose-stimulated insulin secretion. Diabetes. 2007;56:1783–91. [PubMed: 17400930]
33. Eirin A, Zhu XY, Urbieta-Caceres VH, Grande JP, Lerman A, Textor SC and Lerman LO. Persistent kidney dysfunction in swine renal artery stenosis correlates with outer cortical microvascular remodeling. Am J Physiol Renal Physiol. 2011;300:F1394–401. [PubMed: 21367913]

34. Nangaku M, Alpers CE, Pippin J, Shankland SJ, Kurokawa K, Adler S, Morgan BP, Johnson RJ and Couser WG. CD59 protects glomerular endothelial cells from immune-mediated thrombotic microangiopathy in rats. J Am Soc Nephrol. 1998;9:590–7. [PubMed: 9555661]
35. Pipinos II, Nypaver TJ, Moshin SK, Careterro OA and Beierwaltes WH. Response to angiotensin inhibition in rats with sustained renovascular hypertension correlates with response to removing renal artery stenosis. J Vasc Surg. 1998;28:167–77. [PubMed: 9685143]
36. Rihal CS, Textor SC, Breen JF, McKusick MA, Grill DE, Hallett JW and Holmes DR, Jr. Incidental renal artery stenosis among a prospective cohort of hypertensive patients undergoing coronary angiography. Mayo Clin Proc. 2002;77:309–16. [PubMed: 11936924]
37. Imori Y, Akasaka T, Ochiai T, Oyama K, Tobita K, Shishido K, Nomura Y, Yamanaka F, Sugitatsu K, Okamura N, Mizuno S, Arima K, Suenaga H, Murakami M, Tanaka Y, Matsumi J, Takahashi S, Tanaka S, Takeshita S and Saito S. Co-existence of carotid artery disease, renal artery stenosis, and lower extremity peripheral arterial disease in patients with coronary artery disease. Am J Cardiol. 2014;113:30–5. [PubMed: 24157190]
38. Yan JH, Sun LX, Zhao XY, Lian H, Ruan YP, Zhu YL, Zhang SY, Fang Q and Fan ZJ. [Prevalence and risk factors of atherosclerotic renal artery stenosis]. Zhonghua Yi Xue Za Zhi. 2013;93:827–31. [PubMed: 23859388]
39. Colombini M VDAC: the channel at the interface between mitochondria and the cytosol. Mol Cell Biochem. 2004;256–257:107–15.
40. Kaasik A, Safiulina D, Zharkovsky A and Veksler V. Regulation of mitochondrial matrix volume. Am J Physiol Cell Physiol. 2007;292:C157–63. [PubMed: 16870828]
41. Zick M, Rabl R and Reichert AS. Cristae formation-linking ultrastructure and function of mitochondria. Biochim Biophys Acta. 2009;1793:5–19. [PubMed: 18620004]
42. Palikaras K and Tavernarakis N. Mitochondrial homeostasis: the interplay between mitophagy and mitochondrial biogenesis. Exp Gerontol. 2014;56:182–8. [PubMed: 24486129]
43. LeBleu VS, O'Connell JT, Gonzalez Herrera KN, Wikman H, Pantel K, Haigis MC, de Carvalho FM, Damascena A, Domingos Chinen LT, Rocha RM, Asara JM and Kalluri R. PGC-1alpha mediates mitochondrial biogenesis and oxidative phosphorylation in cancer cells to promote metastasis. Nat Cell Biol. 2014;16:992–1003, 1–15. [PubMed: 25241037]
44. Smirnova E, Griparic L, Shurland DL and van der Bliek AM. Dynamin-related protein Drp1 is required for mitochondrial division in mammalian cells. Mol Biol Cell. 2001;12:2245–56. [PubMed: 11514614]
45. Chen H and Chan DC. Mitochondrial dynamics--fusion, fission, movement, and mitophagy--in neurodegenerative diseases. Hum Mol Genet. 2009;18:R169–76. [PubMed: 19808793]
46. Ding WX and Yin XM. Mitophagy: mechanisms, pathophysiological roles, and analysis. Biol Chem. 2012;393:547–64. [PubMed: 22944659]
47. Rubinstein AD and Kimchi A. Life in the balance - a mechanistic view of the crosstalk between autophagy and apoptosis. J Cell Sci. 2012;125:5259–68. [PubMed: 23377657]
48. Cummins TD, Holden CR, Sansbury BE, Gibb AA, Shah J, Zafar N, Tang Y, Hellmann J, Rai SN, Spite M, Bhatnagar A and Hill BG. Metabolic remodeling of white adipose tissue in obesity. Am J Physiol Endocrinol Metab. 2014;307:E262–77. [PubMed: 24918202]
49. Altshuler-Keylin S, Shinoda K, Hasegawa Y, Ikeda K, Hong H, Kang Q, Yang Y, Perera RM, Debnath J and Kajimura S. Beige Adipocyte Maintenance Is Regulated by Autophagy-Induced Mitochondrial Clearance. Cell Metab. 2016;24:402–419. [PubMed: 27568548]
50. Matsuda N, Sato S, Shiba K, Okatsu K, Saisho K, Gautier CA, Sou YS, Saiki S, Kawajiri S, Sato F, Kimura M, Komatsu M, Hattori N and Tanaka K. PINK1 stabilized by mitochondrial depolarization recruits Parkin to damaged mitochondria and activates latent Parkin for mitophagy. J Cell Biol. 2010;189:211–21. [PubMed: 20404107]
51. Zhang T, Xue L, Li L, Tang C, Wan Z, Wang R, Tan J, Tan Y, Han H, Tian R, Billiar TR, Tao WA and Zhang Z. BNIP3 Protein Suppresses PINK1 Kinase Proteolytic Cleavage to Promote Mitophagy. J Biol Chem. 2016;291:21616–21629. [PubMed: 27528605]
52. Li J, Zhao WG, Shen ZF, Yuan T, Liu SN, Liu Q, Fu Y and Sun W. Comparative proteome analysis of brown adipose tissue in obese C57BL/6J mice using iTRAQ-coupled 2D LC-MS/MS. PLoS One. 2015;10:e0119350. [PubMed: 25747866]

53. Bellot G, Garcia-Medina R, Gounon P, Chiche J, Roux D, Pouyssegur J and Mazure NM. Hypoxia-induced autophagy is mediated through hypoxia-inducible factor induction of BNIP3 and BNIP3L via their BH3 domains. Mol Cell Biol. 2009;29:2570–81. [PubMed: 19273585]
54. Okatsu K, Saisho K, Shimanuki M, Nakada K, Shitara H, Sou YS, Kimura M, Sato S, Hattori N, Komatsu M, Tanaka K and Matsuda N. p62/SQSTM1 cooperates with Parkin for perinuclear clustering of depolarized mitochondria. Genes Cells. 2010;15:887–900. [PubMed: 20604804]
55. Bao L, Avshalumov MV, Patel JC, Lee CR, Miller EW, Chang CJ and Rice ME. Mitochondria are the source of hydrogen peroxide for dynamic brain-cell signaling. J Neurosci. 2009;29:9002–10. [PubMed: 19605638]
56. Li Y, Park JS, Deng JH and Bai Y. Cytochrome c oxidase subunit IV is essential for assembly and respiratory function of the enzyme complex. J Bioenerg Biomembr. 2006;38:283–91. [PubMed: 17091399]
57. Gloviczki ML, Glockner JF, Crane JA, McKusick MA, Misra S, Grande JP, Lerman LO and Textor SC. Blood oxygen level-dependent magnetic resonance imaging identifies cortical hypoxia in severe renovascular disease. Hypertension. 2011;58:1066–72. [PubMed: 22042812]
58. Solaini G, Baracca A, Lenaz G and Sgarbi G. Hypoxia and mitochondrial oxidative metabolism. Biochim Biophys Acta. 2010;1797:1171–7. [PubMed: 20153717]
59. Zhang H, Bosch-Marce M, Shimoda LA, Tan YS, Baek JH, Wesley JB, Gonzalez FJ and Semenza GL. Mitochondrial autophagy is an HIF-1-dependent adaptive metabolic response to hypoxia. J Biol Chem. 2008;283:10892–903. [PubMed: 18281291]
60. Czajka A and Malik AN. Hyperglycemia induced damage to mitochondrial respiration in renal mesangial and tubular cells: Implications for diabetic nephropathy. Redox Biol. 2016;10:100–107. [PubMed: 27710853]
61. Wautier MP, Chappey O, Corda S, Stern DM, Schmidt AM and Wautier JL. Activation of NADPH oxidase by AGE links oxidant stress to altered gene expression via RAGE. Am J Physiol Endocrinol Metab. 2001;280:E685–94. [PubMed: 11287350]
62. Eirin A, Zhu XY, Krier JD, Tang H, Jordan KL, Grande JP, Lerman A, Textor SC and Lerman LO. Adipose tissue-derived mesenchymal stem cells improve revascularization outcomes to restore renal function in swine atherosclerotic renal artery stenosis. Stem Cells. 2012;30:1030–41. [PubMed: 22290832]
63. Szeto HH, Liu S, Soong Y, Alam N, Prusky GT and Seshan SV. Protection of mitochondria prevents high-fat diet-induced glomerulopathy and proximal tubular injury. Kidney Int. 2016;90:997–1011. [PubMed: 27519664]
64. Boren J and Brindle KM. Apoptosis-induced mitochondrial dysfunction causes cytoplasmic lipid droplet formation. Cell Death Differ. 2012;19:1561–70. [PubMed: 22460322]
65. Venkatachalam MA and Weinberg JM. Mechanisms of cell injury in ATP-depleted proximal tubules. Role of glycine, calcium, and polyphosphoinositides. Nephrol Dial Transplant. 1994;9 Suppl 4:15–21. [PubMed: 7800249]

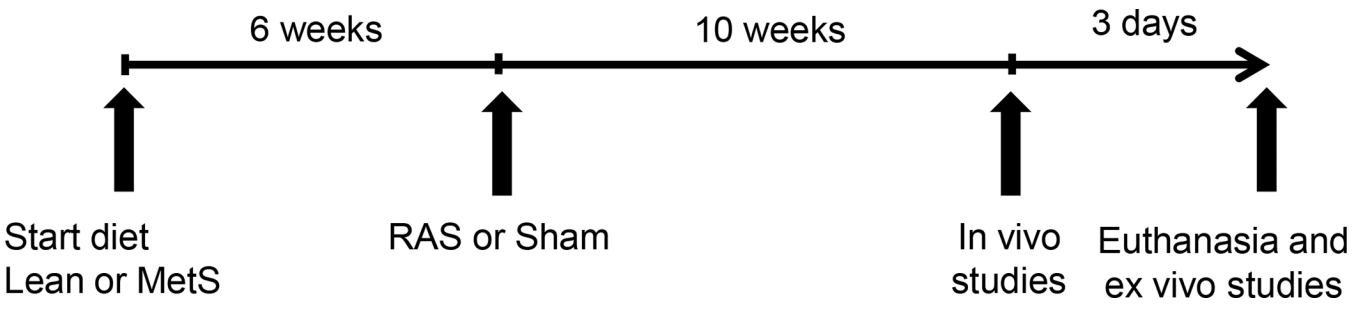

Figure 1. Schematic of the experimental protocol.
MetS: Metabolic syndrome, RAS: Renal artery stenosis.

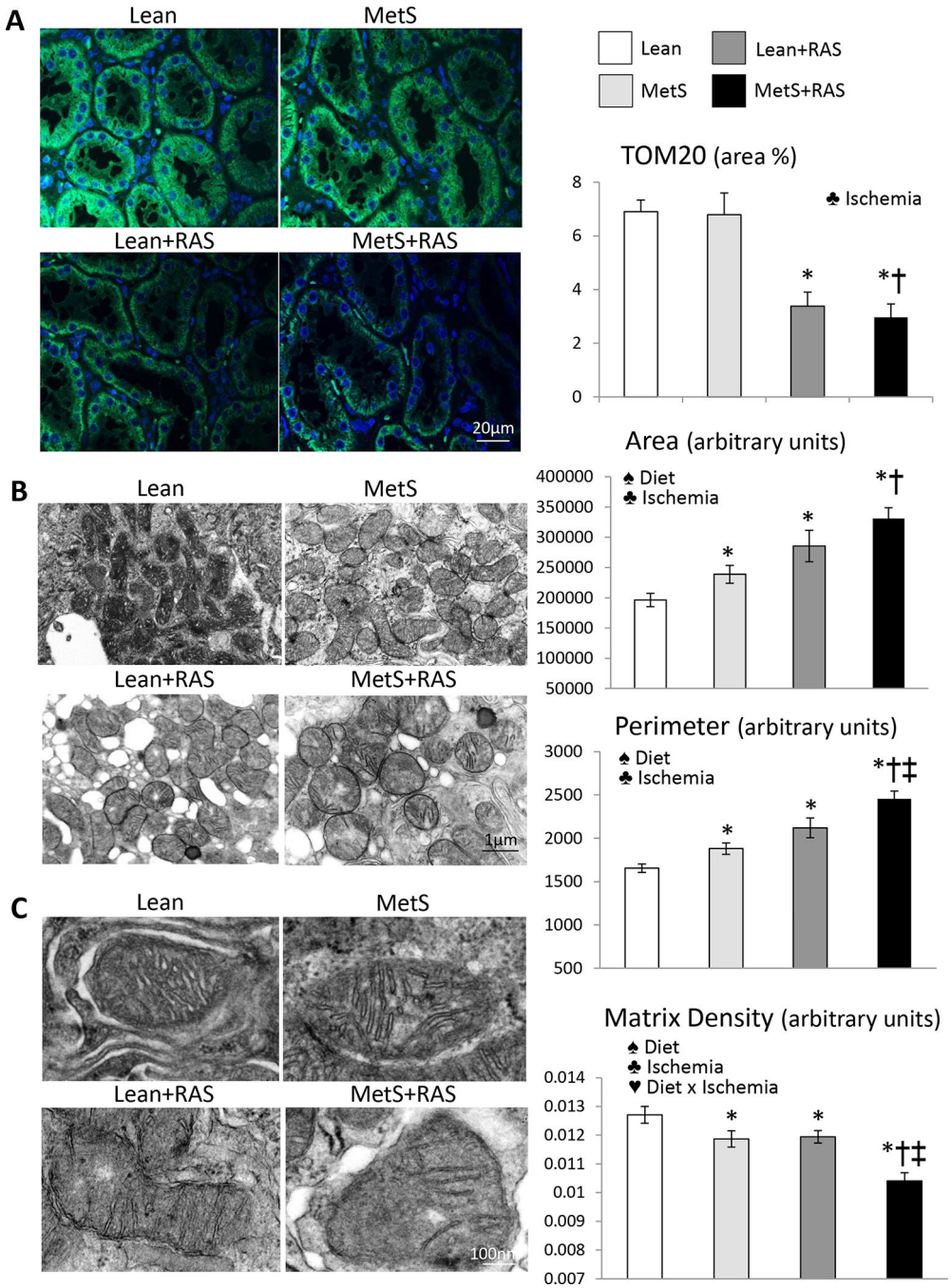

Figure 2. Mitochondrial density and morphology.

A: Representative immunofluorescence staining (original magnification 40X) for the mitochondrial outer membrane marker preprotein translocases of the outer membrane (TOM)-20 (green) showing decreased renal tubular cell mitochondrial density in Lean+RAS and MetS+RAS compared to their respective controls. B: Transmission electron microscopy and quantification of mitochondrial area and perimeter in renal tubular cells in study groups. C: Mitochondrial matrix density decreased in MetS and Lean+RAS compared to Lean, and further decreased in MetS+RAS. *p<0.05 vs. Lean, †p<0.05 vs. MetS, ‡p<0.05 vs. Lean

+RAS. ♠ Diet: Significant effect of MetS diet (2-way ANOVA), ♣ Ischemia: Significant effect of ischemia (2-way ANOVA), ♥ Diet x Ischemia: Significant effect of MetS diet x ischemia (2-way ANOVA).

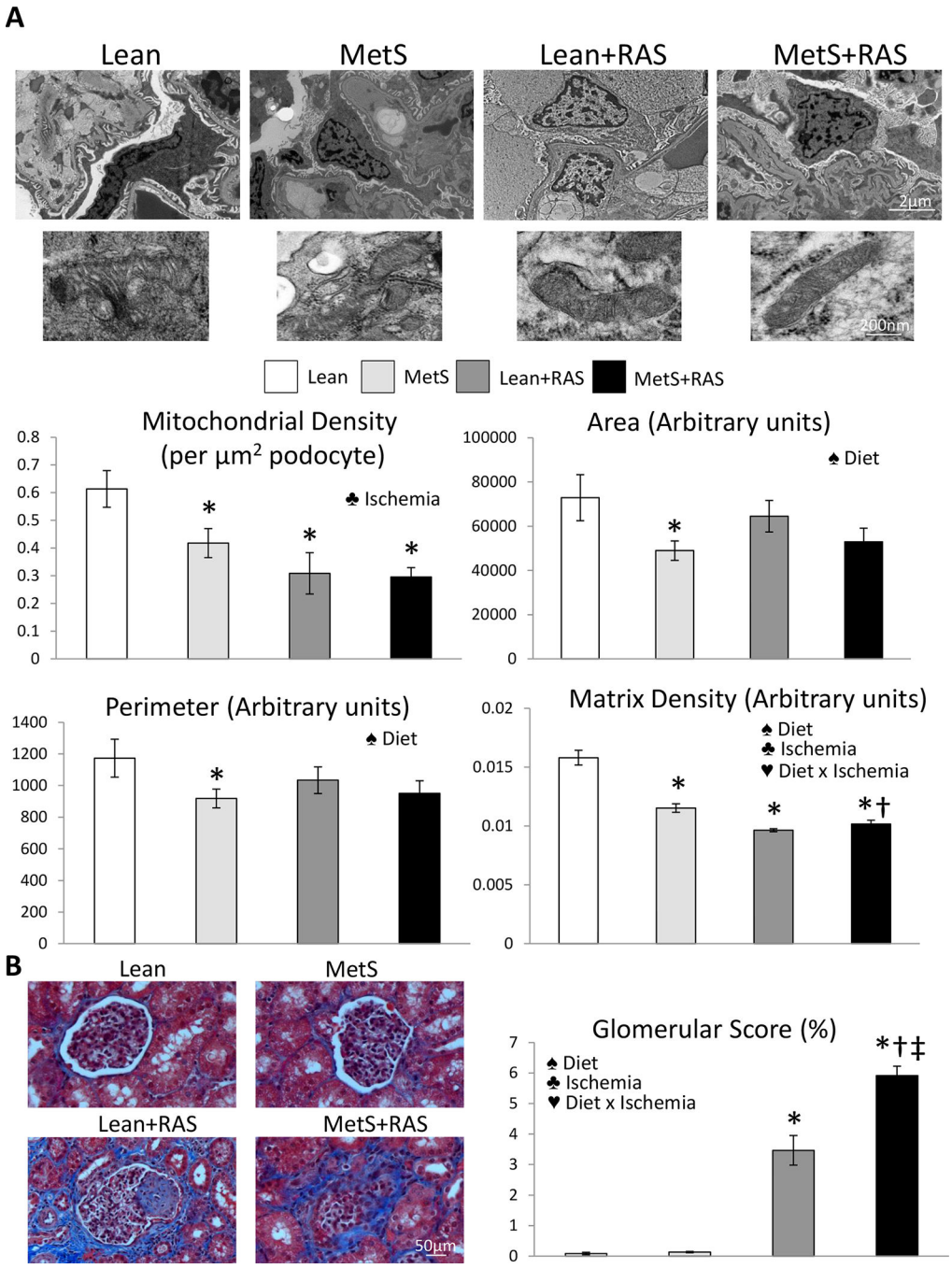

Figure 3. MetS+RAS causes podocyte mitochondrial injury.

A: Representative transmission electron microscopy images of podocytes in all groups. Podocyte mitochondrial density was similarly decreased in MetS, Lean+RAS, and MetS +RAS compared to Lean, and influenced only by ischemia. Mitochondrial area, perimeter, and matrix density were lower in MetS compared to Lean, but the latter further decreased in Lean+RAS and MetS+RAS and was influenced by MetS diet, ischemia, and their interaction. B: Glomerular score was higher in Lean+RAS versus Lean and MetS, further increased in MetS+RAS, and was influenced by MetS diet, ischemia, and their interaction.

*p<0.05 vs. Lean, †p<0.05 vs. MetS, ‡p<0.05 vs. Lean+RAS. ♠ Diet: Significant effect of MetS diet (2-way ANOVA), ♣ Ischemia: Significant effect of ischemia (2-way ANOVA), ♥ Diet x Ischemia: Significant effect of MetS diet x ischemia (2-way ANOVA).

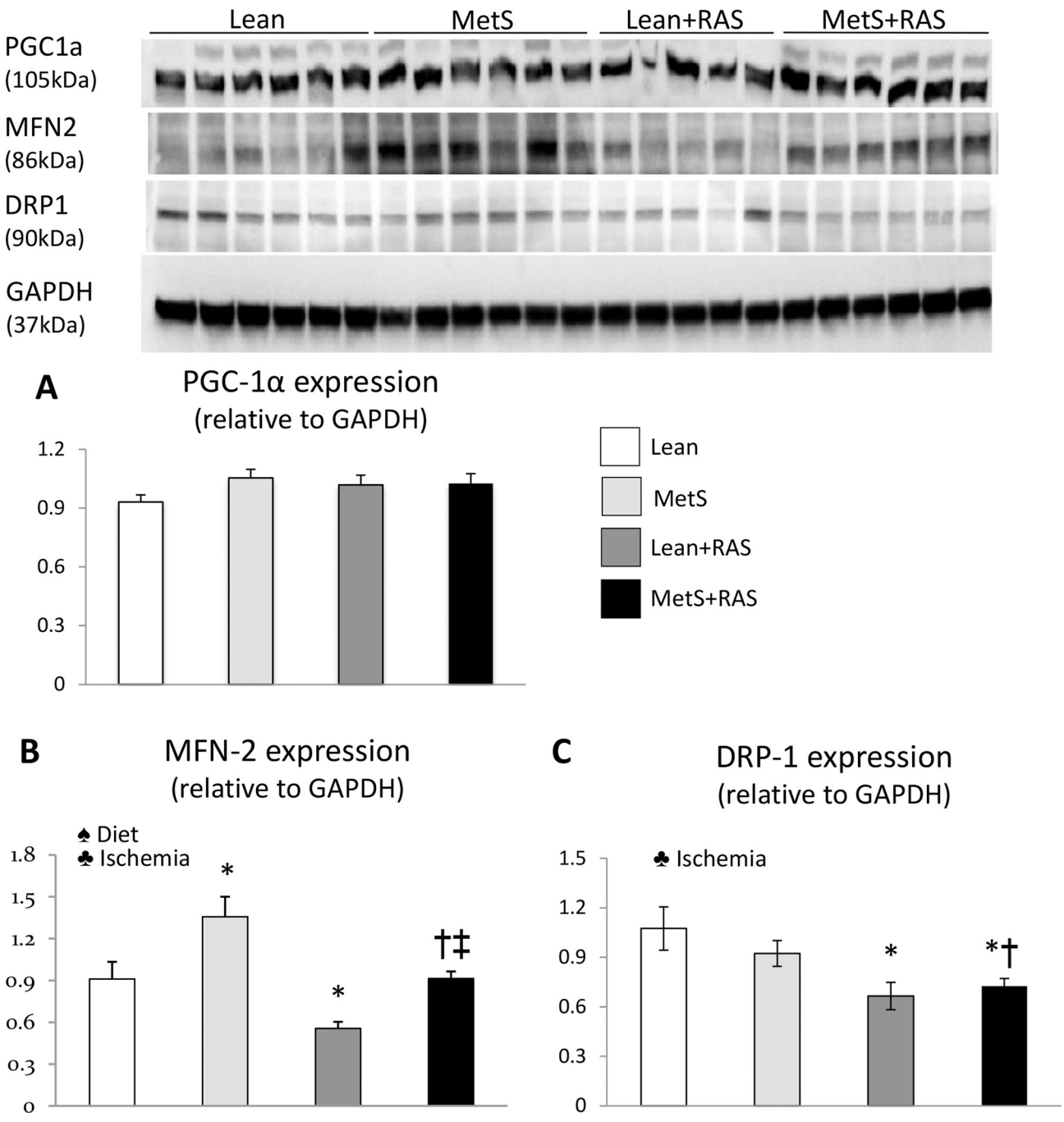

Figure 4. Mitochondrial homeostasis.

A: Renal protein expression of peroxisome-proliferator-activated receptor γ co-activator (PGC)-1α (A), mitofusin (MFN)-2 (B), and dynamin-related protein (DRP)-1 (C) in study groups. *p<0.05 vs. Lean, †p<0.05 vs. MetS, ‡p<0.05 vs. Lean+RAS. ♠ Diet: Significant effect of MetS diet (2-way ANOVA), ♣ Ischemia: Significant effect of ischemia (2-way ANOVA).

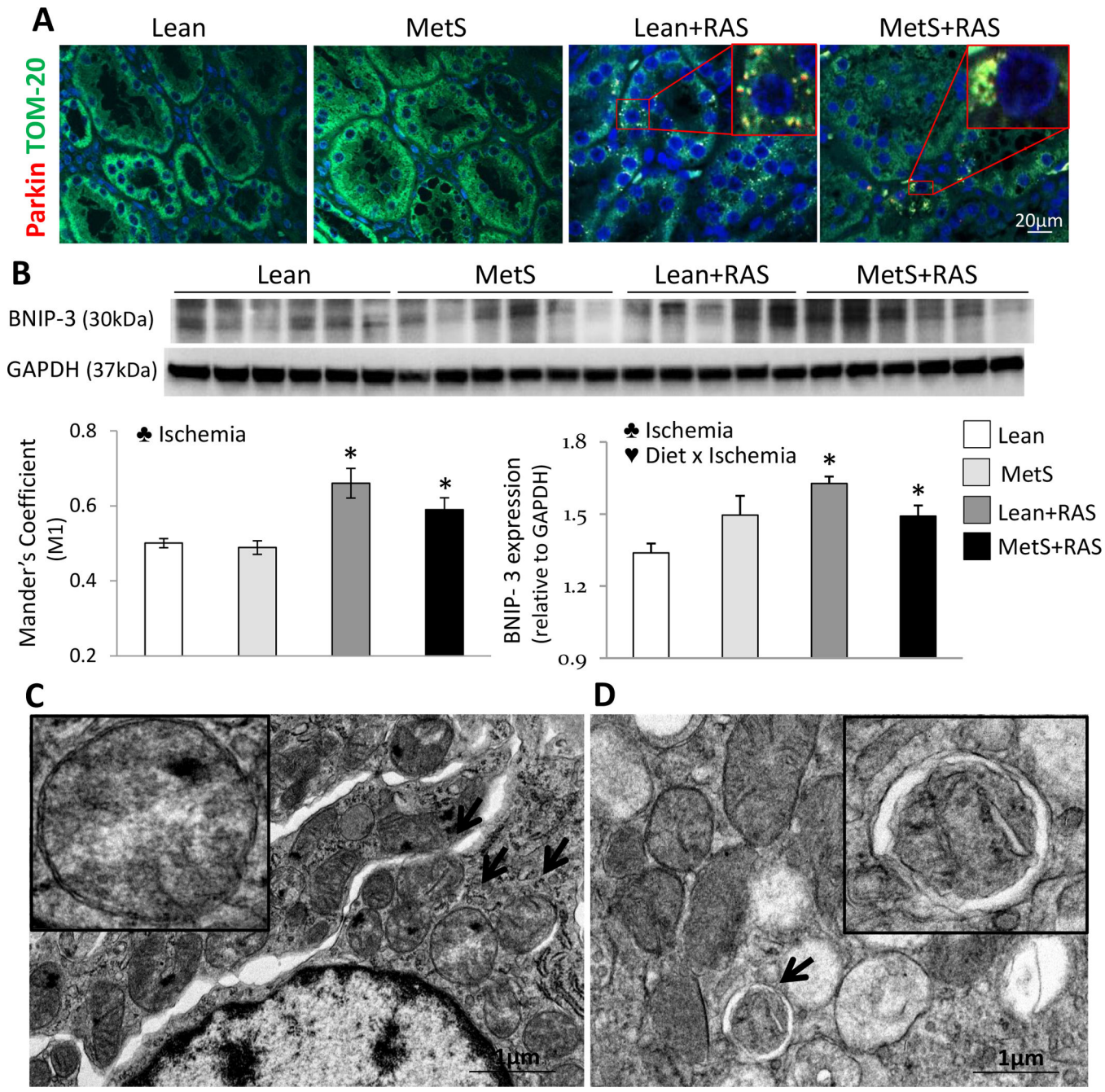

Figure 5. Mitophagy.

A: Representative renal immunofluorescence staining for TOM-20 (green) and Parkin (red), and their co-localization. B: Renal protein expression of BCL2/adenovirus E1B 19kDa protein-interacting protein (BNIP)-3 in study groups. C: Transmission electron microscopy showing perinuclear clusters of structurally damaged mitochondria (arrows) in renal tubular cells from MetS+RAS pigs. D: Representative autophagic structure (mitophagosome) containing a damaged mitochondrion (arrow) in MetS+RAS tubular cells. *p<0.05 vs. Lean, †p<0.05 vs. MetS, ‡p<0.05 vs. Lean+RAS. ♣ Ischemia: Significant effect of ischemia (2-

way ANOVA), ♥ Diet x Ischemia: Significant effect of MetS diet x ischemia (2-way ANOVA).

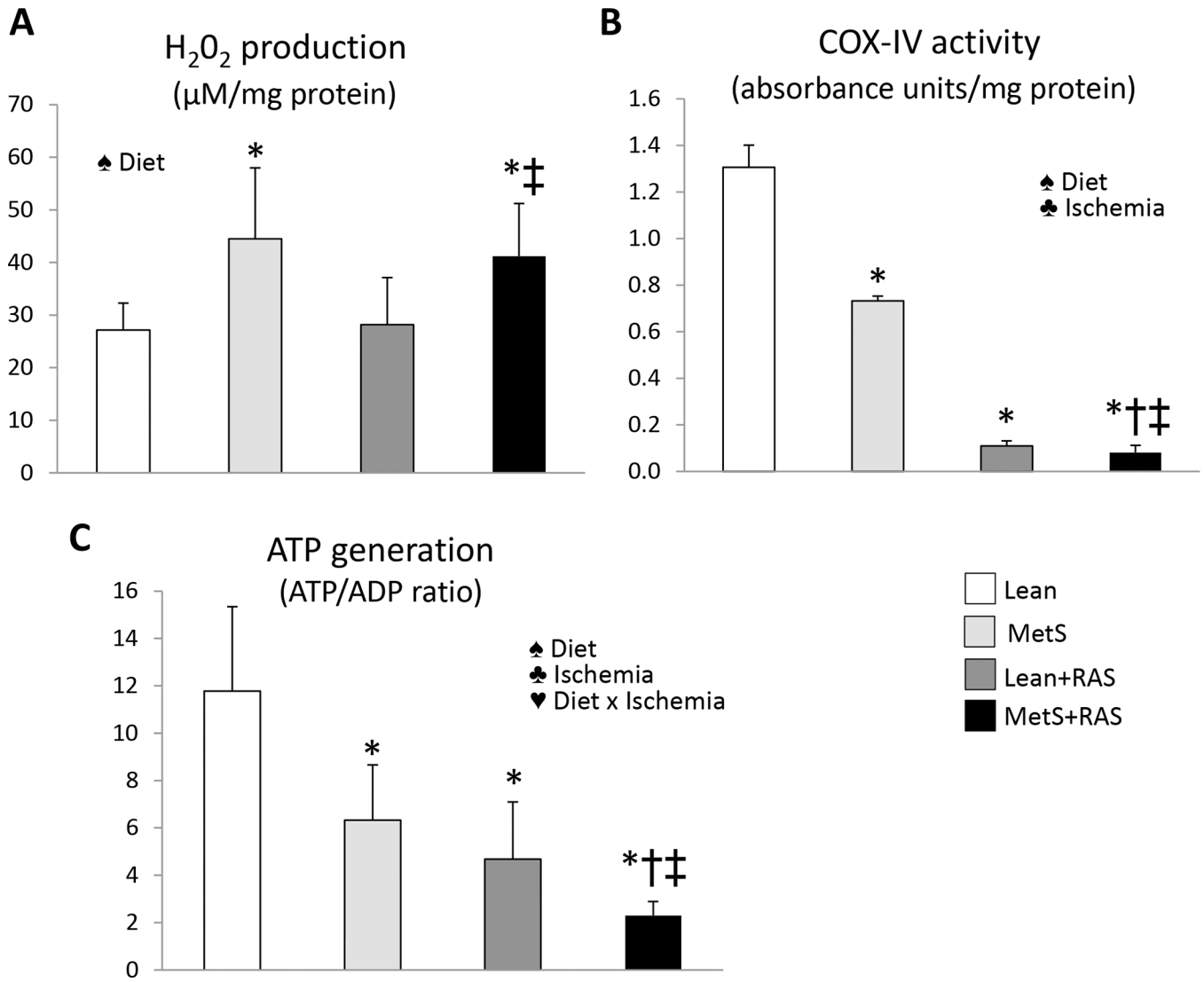

Figure 6. Mitochondrial dysfunction.

A: Mitochondrial hydrogen peroxide (H_20_2) similarly increased in MetS and MetS+RAS compared to their respective controls. B: Cytochrome-c oxidase (COX)-IV activity decreased in MetS compared to Lean and in Lean+RAS versus MetS, and further decreased MetS+RAS. C: Mitochondrial ATP production ratio similarly decreased in MetS and Lean +RAS compared to Lean, and further decreased in MetS+RAS. *p<0.05 vs. Lean, †p<0.05 vs. MetS, ‡p<0.05 vs. Lean+RAS.

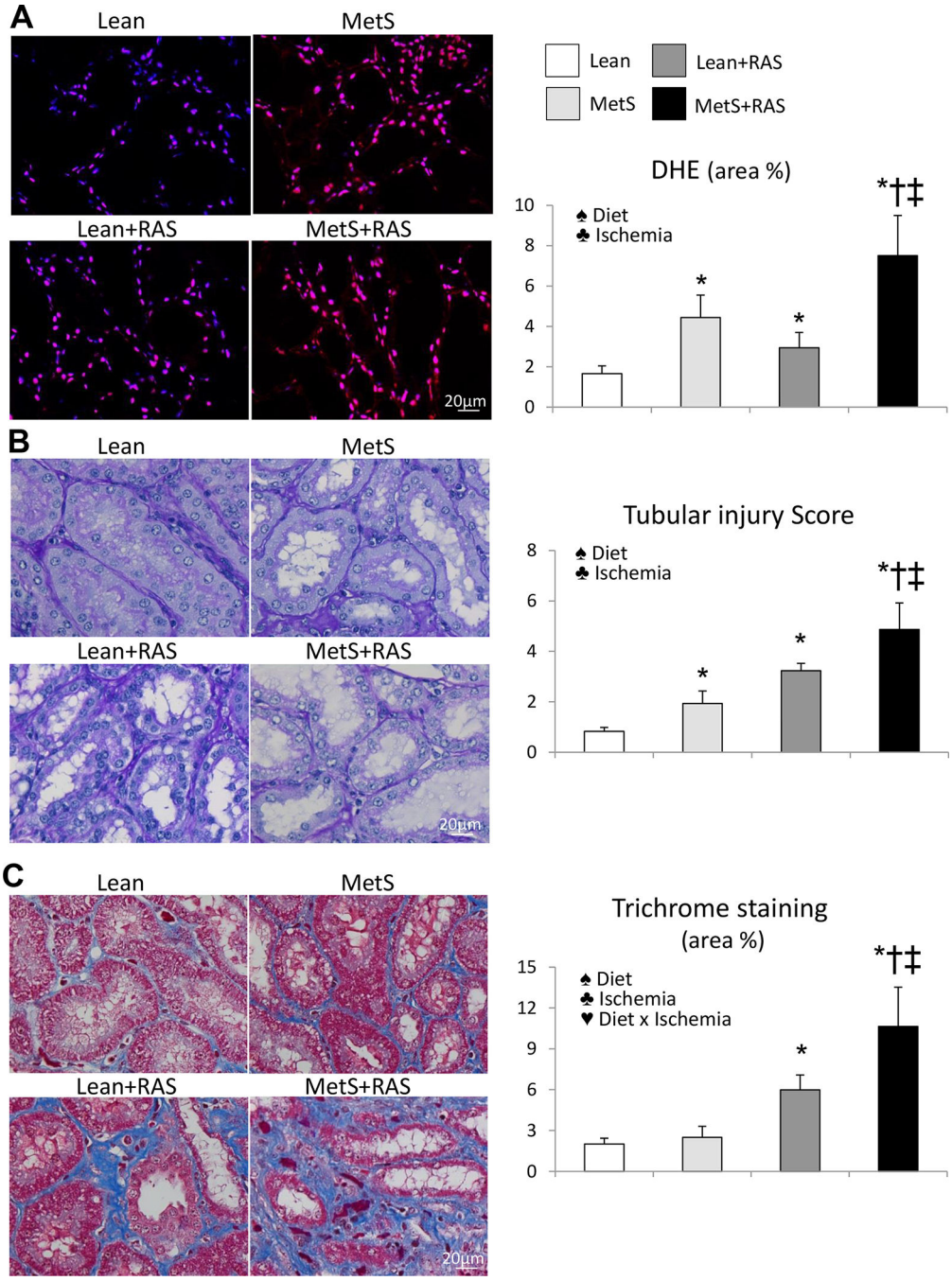

Figure 7. Renal injury in MetS+RAS.

A: Representative kidney dihydroethidium (DHE, red) staining (40X) and its quantification. B: Periodic acid-Schiff staining (40X), showing increased renal tubular injury in MetS compared to Lean, which increased in Lean+RAS, and further increased in MetS+RAS. C: Tubulointerstitial fibrosis (trichrome staining) increased in Lean+RAS compared to Lean and MetS, and further increased in MetS+RAS. *p<0.05 vs. Lean, †p<0.05 vs. MetS, ‡p<0.05 vs. Lean+RAS. ♠ Diet: Significant effect of MetS diet (2-way ANOVA), ♣

Ischemia: Significant effect of ischemia (2-way ANOVA), ♥ Diet x Ischemia: Significant effect of MetS diet x ischemia (2-way ANOVA).

J Hypertens. Author manuscript; available in PMC 2019 October 01.

Table 1.

Baseline characteristics and single-kidney function in study groups (n=6 each).

	Lean	MetS	Lean+RAS	MetS+RAS	p-value for Two-Way ANOVA		
					Diet	Ischemia	Diet × Ischemia
Body weight (Kg)	52.5 ± 1.1	94.0 ± 0.8 *	50.2 ± 1.4	91.6 ± 1.2 *≠	<0.001	0.96	0.93
MAP (mmHg)	102.1 ± 4.2	119.8 ± 5.5 *	125.5 ± 9.0 *	121.2 ± 5.9 *	0.32	0.07	0.11
Degree of stenosis (%)	0	0	71.7 ± 10.5	68.2 ± 6.0	0.78	<0.001	0.78
Total cholesterol (mg/dl)	83.6 ± 2.4	442.6 ± 28.5 *	80.2 ± 2.4	408.1 ± 34.4 *≠	<0.001	0.49	0.57
LDL cholesterol (mg/dl)	34.7 ± 2.4	347.5 ± 58 *	32.4 ± 2.5	336.4 ± 38.6 *≠	<0.001	0.85	0.90
Triglycerides (mg/dl)	8.3 ± 0.9	16.8 ± 2.0 *	8.3 ± 0.7	13.7 ± 1.2 *≠	<0.001	0.26	0.26
Fasting insulin (mU/ml)	0.4 [0.4–0.5]	0.7 [0.7–0.75] *	0.4 [0.4–0.5]	0.7 [0.7–0.8] *≠	<0.001	0.63	0.63
HOMA-IR score	0.65 [0.6–0.7]	1.9 [1.8–1.9] *	0.6 [0.6–0.7]	1.8 [1.7–1.9] *≠	<0.001	0.64	0.76
Fasting glucose (mg/dl)	123.7 ± 5.8	113.3 ± 6.8	121.3 ± 12.1	110.3 ± 9.0	0.25	0.77	0.97
Serum creatinine (mg/dl)	1.22 ± 0.07	1.34 ± 0.09	1.61 ± 0.04 *	1.92 ± 0.07 *†≠	<0.01	<0.001	0.18
ACR(mg/g)	1.7 ± 0.5	1.3 ± 0.5	5.7 ± 1.0 *	4.8 ± 0.1 *	0.17	<0.001	0.42
PRA (ng/ml/h)	0.11 [0.01–0.17]	0.17 [0.09–0.24]	0.24 [0.01–0.3]	0.16 [0.04–0.22]	0.71	0.97	0.33
Renal volume (ml)	135.6 ± 7.4	218.8 ± 8.7 *	78.3 ± 7.4 *	187.0 ± 8.8 *†≠	<0.001	<0.001	0.16
RBF (ml/min)	503.5 ± 32.4	839.1 ± 89.4 *	315.8 ± 23.6 *	653.6 ± 13.0 *†≠	<0.001	<0.01	0.59
GFR (ml/min)	74.3 ± 4.2	140.5 ± 8.3 *	45.2 ± 3.7 *	103.7 ± 7.3 *†≠	<0.001	<0.005	0.93
Renal volume to BW (ml/Kg)	2.0 ± 0.1	2.3 ± 0.1 *	1.6 ± 0.2 *	2.0 ± 0.1†≠	<0.01	<0.01	0.91
RBF to BW (ml/min/Kg)	7.3 ± 0.6	9.0 ± 0.9 *	6.0 ± 0.5 *	7.0 ± 0.2†≠	<0.05	<0.05	0.59
GFR to BW (ml/min/Kg)	1.1 ± 0.1	1.5 ± 0.1 *	0.9 ± 0.1 *	1.1 ± 0.1†≠	<0.001	<0.001	0.24

MetS: metabolic syndrome, RAS: renal artery stenosis, MAP: mean arterial pressure, LDL: low-density lipoprotein, HOMA-IR: homeostasis model assessment of insulin resistance, ACR: albumin creatinine ratio, PRA: plasma renin activity, RBF: renal blood flow, GFR: glomerular filtration rate, BW: Body weight.

* p<0.05 vs. Lean;

≠ p<0.05 vs. Lean+RAS.